JURNAL KARTIKA KIMIA

J. Kartika Kimia, May 2025, 8, (1), 1-10
Journal homepage: http://jkk.unjani.ac.id/index.php/jkk
P-ISSN: 2655-1322 E-ISSN: 2655-0938

Catalytic Liquid-phase Oxidation of Phenol under Mild Condition over Pt/CeO_2–ZrO_2–SnO_2/SBA-16: Loading Optimization and Kinetic Analysis

Abdul Rohman Supandi[1,2*], Naoyoshi Nunotani[2], Nobuhito Imanaka[2,†]
[1]Division of Inorganic and Physical Chemistry, Faculty of Mathematics and Natural Sciences, Institut Teknologi Bandung, Jl. Ganesha No. 10, Bandung 40132, Indonesia
[2]Department of Applied Chemistry, Faculty of Engineering, Osaka University, Osaka, Japan
2-1 Yamadaoka, Suita, Osaka 565-0871 Japan
[†]Present: Professor Emeritus, Osaka University, Osaka, Japan
*E-mail: abdulrohman.s@itb.ac.id

DOI: https://doi.org/10.26874/jkk.v8i1.921

Received: 15 May 2025, *Revised*: 7 June 2025, *Accepted*: 7 June 2025, *Online*: 9 June 2025

Abstract

Phenol removal through catalytic liquid-phase oxidation using oxygen gas is a green and efficient method. This study reports a systematic investigation of Pt catalysts supported on CeO_2–ZrO_2–SnO_2/SBA-16, focusing on the effect of SnO_2 doping as well as CeO_2–ZrO_2–SnO_2 and Pt loading as a comprehensive strategy to tune catalytic performance under mild conditions. This approach offers a more integrated optimization of catalyst structure and composition, leading to enhanced activity and new mechanistic insights into phenol removal over multicomponent oxide-supported Pt catalysts. XRD and H_2-TPR analyses confirmed that 15 mol% Sn ($Ce_{0.68}Zr_{0.17}Sn_{0.15}O_2$) provided optimal redox behavior, while higher Sn content led to phase separation. Catalytic tests at 80 °C and atmospheric pressure showed that 7 wt% Pt/ 16 wt% $Ce_{0.68}Zr_{0.17}Sn_{0.15}O_2$/SBA-16 achieved the highest phenol removal (91%). Increasing CeO_2-ZrO_2-SnO_2 loading up to 16 wt% improved activity, though further increase reduced surface area and performance. Meanwhile, Pt loading was optimal at 7 wt%. Kinetic analysis revealed the reaction followed pseudo-first-order kinetics with a rate constant of 0.39 h^{-1}. The activation energy, derived from Arrhenius plots, was 57.7 $kJ \cdot mol^{-1}$. These findings demonstrate that optimized CeO_2-ZrO_2-SnO_2 and Pt loadings significantly enhance phenol oxidation under mild conditions, offering a promising route for effective wastewater treatment.

Keywords: Catalytic phenol oxidation, CeO_2–ZrO_2–SnO_2, Kinetic analysis, Loading optimization

1 Introduction

Growing environmental concerns play a crucial role in promoting sustainable development within the industrial sector, which often generates hazardous byproducts and excess raw materials. A significant number of organic pollutants originating from industrial activities are released into wastewater streams. Among these, phenol is a particularly prevalent contaminant due to its extensive use as a precursor in the manufacturing of various chemicals such as phenolic resins, bisphenol A, salicylic acid, and caprolactam [1-3]. Unfortunately, phenol poses serious health risks to humans, potentially affecting the heart, central nervous system, and kidneys [4-5]. It is also known to be extremely toxic to aquatic organisms [6-8]. Consequently, developing an effective and practical method for phenol removal is essential.

Liquid phase oxidation using heterogeneous catalysts is a phenol removal method that offers many benefits, such as an easy recovering procedure and environmentally friendly [9-12]. However, many recent methods rely on additional oxidants like H_2O_2 [13] or peroxymonosulfate [14], which complicate real-world applications. In contrast, catalytic wet air oxidation (CWAO) using molecular oxygen is safer and more practical. For this purpose, platinum catalyst supported on CeO_2–ZrO_2 solid solution has attracted significant attentions, because the catalyst exhibited good catalytic performance in phenol oxidation [10-12]. CeO_2–ZrO_2 solid solution has high oxygen storage capacity as well as good thermal and chemical stability with cubic fluorite-type structure [15-17]. In this catalyst, CeO_2–ZrO_2 functions as an oxygen promoter for platinum, attributed to the facile and reversible

redox behavior of the Ce^{4+}/Ce^{3+} couple ion [18]. Nevertheless, the catalyst still requires arduous reaction condition to remove the phenol, such as elevated temperatures (around 160 °C) and high partial pressure oxygen gas (up to 2 MPa) [10-12]. Therefore, there is still a need to develop an efficient catalytic system capable of removing phenol at moderate temperatures (<100 °C) and at ambient pressure.

To improve catalytic performance under milder conditions, our previous study doped SnO_2 into the CeO_2–ZrO_2 support system [19,20]. The resulting Pt/CeO_2–ZrO_2–SnO_2/SBA-16 catalyst showed better performance for phenol removal compared to Pt/CeO_2–ZrO_2/SBA-16, highlighting the beneficial role of SnO_2 in enhancing redox behavior and oxygen mobility [21]. In this system, SBA-16 was employed as a mesoporous silica support due to its high surface area and three-dimensional pore structure, which facilitate uniform dispersion of active components and improve mass transport.

However, despite these promising results, several key questions remain unaddressed. Previous studies often explored catalyst compositions in a limited or empirical manner, without systematically investigating the effect of SnO_2 doping levels, the optimal loading of multicomponent oxide supports, or the influence of Pt content on both structural and catalytic properties. Furthermore, the reaction kinetics by using the catalyst also remains insufficiently understood. These gaps hinder the rational design of more efficient catalysts for phenol oxidation and similar liquid-phase oxidation reactions. Building upon our earlier findings, the present study aims to address these shortcomings through a comprehensive optimization of the Pt/CeO_2–ZrO_2–SnO_2/SBA-16 catalyst. Specifically, we examine the effects of SnO_2 content, CeO_2–ZrO_2–SnO_2 support loading, and Pt loading on catalytic activity under moderate reaction conditions. In addition, we conduct kinetic analysis to quantify the reaction rate and the activation energy. This approach offers new perspective into the design of effective catalysts for sustainable wastewater treatment.

2 Method

2.1 Catalyst preparation

The mesoporous silica support, SBA-16, was synthesized via a modified hydrothermal approach based on previously reported methods [22,23]. Initially, 1.6 g of Pluronic F-127 was dissolved in 90 mL of 0.2 mol L^{-1} hydrochloric acid. After complete dissolution, 1.1 mL of 1,3,5-trimethylbenzene was introduced into the solution, followed by stirring at 35 °C for 3 hours to facilitate micelle formation. Subsequently, 7.1 mL of tetraethyl orthosilicate (TEOS) was added, and the mixture was stirred continuously for 20 hours. The resulting gel was poured into a Teflon-lined autoclave and underwent hydrothermal processing at 140 °C for 24 hours. The result was filtrated to obtain a solid product and then dried at ambient temperature followed by calcination at 400 °C for 4 hours in air (flow rate: 20 mL min^{-1}) to remove the template and obtain the final SBA-16 material.

A CeO_2–ZrO_2–SnO_2 solid was loaded onto SBA-16 using a co-precipitation method to obtain a composite with various doping amount of SnO_2 and loading amount of CeO_2–ZrO_2–SnO_2 by mixing certain amount of precursors of 1.0 mol L^{-1} $Ce(NO_3)_3$, 0.1 mol L^{-1} $ZrO(NO_3)_2$, and SnC_2O_4 powder to form x wt% $Ce_{0.8(1-a)}Zr_{0.2(1-a)}Sn_aO_2$/ SBA-16 composites (**see Table S1 and S2**). This solution was stirred at room temperature for 30 minutes to ensure homogeneity before adding SBA-16 powder. After the addition, the suspension was stirred for another 30 minutes. The pH was gradually adjusted to 11 using a 5.6% aqueous ammonia solution, followed by continuous stirring for 12 hours. The resulting solid was separated by filtration and calcined at 900 °C for 1 hour. Hereafter, these x wt% $Ce_{0.8(1-a)}Zr_{0.2(1-a)}Sn_aO_2$/ SBA-16 composites are denoted as CZSn$_a$$x$SBA.

Platinum was introduced into the composite by an impregnation technique using a Pt precursor stabilized in ethanol with polyvinylpyrrolidone (Pt-PVP, Pt: 4.0 wt%). The Pt precursor was mixed added to the dispersed x wt% $Ce_{0.8(1-a)}Zr_{0.2(1-a)}Sn_aO_2$/SBA-16 composite in water to form y wt% Pt/ x wt% $Ce_{0.8(1-a)}Zr_{0.2(1-a)}Sn_aO_2$/ SBA-16 ($y$ = 0, 1, 3, 7, 10). The mixture was stirred for 6 hours at room temperature to ensure uniform distribution of Pt, followed by solvent evaporation at 180 °C. The resulting material was then calcined at 500 °C for 4 hours to obtain the final catalyst. Hereafter, y wt% Pt/ x wt% $Ce_{0.8(1-a)}Zr_{0.2(1-a)}Sn_aO_2$/ SBA-16 catalyst are denoted as PtyCZSn$_a$$x$SBA.

2.2 Catalyst characterization

The prepared catalysts were measured by X-ray diffraction (XRD; SmartLab, Rigaku) with Cu-Kα radiation in the 2θ range 10–70°. Elemental compositions were analyzed by X-ray fluorescence spectroscopy (XRF, Supermini 200,

Rigaku) to verify the actual loading of Ce, Zr, Sn, and Pt in the catalysts. The specific surface area was evaluated by nitrogen adsorption–desorption measurements at −196 °C using a Tristar 3000 surface analyzer (Shimadzu) and the Brunauer–Emmett–Teller (BET) method was used to determine surface area. To assess the redox properties of the catalysts, temperature-programmed reduction (TPR) analysis was conducted under a 5 vol% H_2/Ar gas mixture (flow rate: 50 mL min^{-1}) with a heating rate of 5 °C min^{-1}, using a Belcat-B instrument (MicrotracBel).

2.3 *Catalytic test*

The oxidation reaction of phenol was carried out in the oil bath using a 300 cm^3 three necked flask equipped with an opened condenser at 80 °C in atmospheric pressure and magnetically stirred (500 rpm). An aqueous solution of phenol 1000 ppm (10 mL) and the catalyst (0.4 g) were mixed in the flask. After the preset reaction time, the aliquot was collected through the centrifugation process (Allegra 64R centrifuge, Beckman Coulter). The samples were then mixed with naphthalene solution in methanol (1000 ppm) for gas chromatography-mass spectrometry (GC-MS; GCMS-QP2010 Plus, Shimadzu) measurement to evaluate the phenol removal percentage and investigate the presence of intermediate compounds. The phenol removal percentage was calculated using **Eq. 1**.

$$Phenol\ removal\ percentage = \frac{C_0 - C}{C_0} x100\% \quad \text{(Equation 1)}$$

where, C_0 and C are phenol initial concentration and phenol concentration after reaction, respectively.

Additionally, the rate constant (k) and activation energy of catalysts were also investigated by plotting the $-\ln[C/C_0]$ vs. the reaction time (t) and using the Arrhenius equation, respectively. The rate constant (k) was calculated following pseudo-first-order reaction and continued to investigate the activation energy (E_a) using the following **Eq. 2** and **Eq. 3**.

$$\frac{dC}{dt} = kC_0 \quad \text{(Equation 2)}$$

$$k = A\, e^{-E_a/RT} \quad \text{(Equation 3)}$$

where A, R, and T are the pre-exponential factor, the gas constant, and the reaction temperature, respectively.

3 Result and Discussion

3.1 *The effect of SnO_2 doping amount on the performance of catalyst*

To examine the effect of SnO_2 content on the catalyst structure, a series of Pt-supported catalysts were synthesized with SnO_2 molar ratios of 0.05, 0.10, 0.15, 0.20, and 0.25 relative to the total metal oxides. Here, the Pt and $Ce_{0.8(1-a)}Zr_{0.2(1-a)}Sn_aO_2$ loading amount were fixed to be 7 wt% and 16 wt%, respectively. The composition of the prepared catalysts was in good agreement with the feed composition that confirmed by the XRF measurement as shown in **Table 1**. **Fig. 1** presents the XRD patterns of the Pt7CZSn$_a$16SBA series. For the catalysts with $a \leq 0.20$, the diffraction patterns exhibit reflections corresponding only to the SBA-16 mesostructure, the cubic fluorite-type phase typical of CeO_2–ZrO_2, and metallic Pt. Notably, no obvious peaks attributable to SnO_2 are detected, suggesting that Sn^{4+} ions were successfully incorporated into the CeO_2–ZrO_2 lattice without forming a separate crystalline phase. Moreover, a subtle shift in the cubic fluorite-type diffraction peaks is observed with increasing SnO_2 content up to a = 0.15, particularly evident in the magnified XRD region between 2θ = 25–35°. This shift can be attributed to the partial substitution of Ce^{4+} (ionic radius = 0.111 nm) and Zr^{4+} (0.098 nm) by the slightly smaller Sn^{4+} ion (0.095 nm) [24], which causes lattice contraction and confirms the successful doping of Sn^{4+} into the fluorite lattice. Further shift was not observed for a = 0.20 compared with a = 0.15, meaning that a = 20 may contain an impurity such as amorphous tin dioxide.

Table 1 The measured composition of the prepared 7.0wt%Pt/16.0wt%$Ce_{0.8(1-a)}Zr_{0.2(1-a)}Sn_aO_2$/SBA-16 (Pt7CZSn$_a$16SBA) catalysts with different a

a	Measured composition
0.05	7.3wt%Pt/16.8wt%$Ce_{0.75}Zr_{0.18}Sn_{0.07}O_2$/SBA-16
0.10	7.2wt%Pt/17.1wt%$Ce_{0.71}Zr_{0.17}Sn_{0.12}O_2$/SBA-16
0.15	6.8wt%/Pt/16.4wt%$Ce_{0.69}Zr_{0.17}Sn_{0.14}O_2$/SBA-16
0.20	7.2wt%Pt/15.4wt%$Ce_{0.65}Zr_{0.16}Sn_{0.19}O_2$/SBA-16
0.25	7wt%Pt/16wt%$Ce_{0.6}Zr_{0.15}Sn_{0.25}O_2$/SBA-16

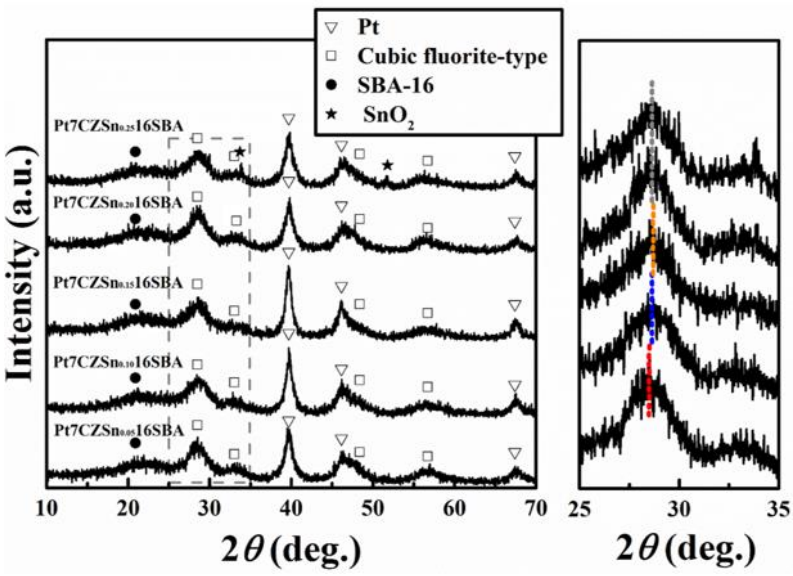

Figure 1 XRD patterns of Pt7Ce$_{0.8(1-a)}$Zr$_{0.2(1-a)}$Sn$_a$O$_2$16SBA catalysts

In contrast, the XRD patterns of the catalyst with higher SnO_2 doping (a = 0.25) show additional peaks corresponding to crystalline SnO_2. This indicates that while some Sn^{4+} ions were still incorporated into the CeO_2–ZrO_2 lattice (as evidenced by the continued peak shift), excess SnO_2 began to segregate and form a distinct crystalline phase at higher loading levels. These results suggest a solubility limit for Sn^{4+} in the CeO_2–ZrO_2 solid solution under the present synthesis conditions.

The H_2-temperature programmed reduction (H_2–TPR) profiles of CZSn$_{0.05}$16SBA, CZSn$_{0.1}$16SBA, CZSn$_{0.15}$16SBA, and CZSn$_{0.2}$16SBA are presented in Fig. 2. Meanwhile, CZSn$_{0.25}$16SBA was excluded from further analysis because the impurity phase of crystalline SnO_2 was unambiguously observed. There are two peaks identified as the surface and bulk reductions at lower and higher temperatures, respectively. As the SnO_2 doping level increased from a mole ratio of 0.05 to 0.15, a progressive shift of the reduction peaks toward lower temperatures was observed. This trend indicates enhanced redox behavior, attributable to improved reducibility of Ce^{4+} to Ce^{3+} facilitated by the presence of Sn^{4+}. The incorporation of SnO_2 into the CeO_2–ZrO_2 lattice likely promotes the formation of oxygen vacancies associated with both the Ce^{4+}/Ce^{3+} and Sn^{4+}/Sn^{2+} redox pairs and the simultaneous reduction of Ce^{4+} and Sn^{4+} in the CeO_2-ZrO_2-SnO_2, which together enhance the material's ability to store and release oxygen during catalytic cycles [19, 25–28]. In the case of CZSn$_{0.2}$16SBA, an increase in surface reduction temperature was observed compared to CZSn$_{0.15}$16SBA. This phenomenon may be attributed to the amorphous tin dioxide impurity.

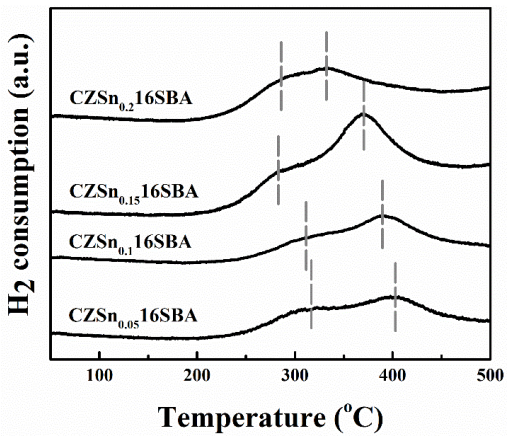

Figure 2 H_2–TPR profiles of CZSn$_a$16SBA

Fig. 3 presents the phenol removal performance of Pt7CZSn$_a$16SBA catalysts (x = 0.05, 0.10, 0.15, 0.20) after 6 hours of reaction at 80 °C under atmospheric pressure. The catalytic activity increased with the SnO_2 doping level, reaching a maximum at a Sn mole ratio of 0.15. At this optimal composition (Pt7CZSn$_{0.15}$16SBA), the phenol removal percentage reached approximately 91%, as previously reported [21]. This improvement is consistent with the H_2–TPR results (**Fig. 2**), where Pt7CZSn$_{0.15}$16SBA exhibited the lowest surface reduction temperature, signifying the most favorable redox properties. Enhanced redox behavior facilitates more efficient oxygen activation and transfer, which is critical for catalytic oxidation. However,

further increasing the SnO_2 content to a mole ratio of 0.20 led to a decline in phenol removal efficiency.

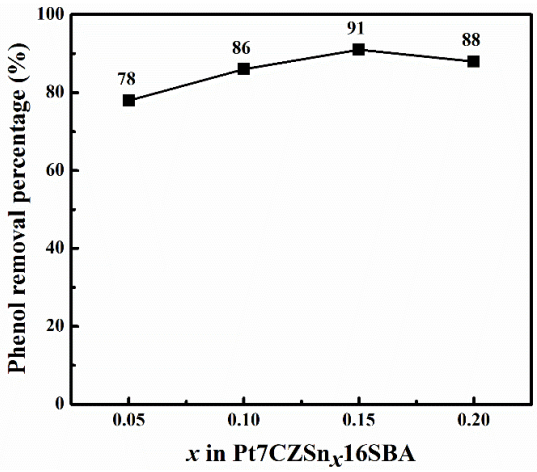

Figure 3 Phenol removal percentage after reaction using Pt7CZSn$_a$16SBA catalysts

3.2 *The effect of CeO_2–ZrO_2–SnO_2 loading amount on the performance of catalyst*

Following the optimization of SnO_2 doping within the CeO_2–ZrO_2–SnO_2 lattice, further investigation was conducted by varying the overall loading amount of the CZSn$_{0,15}$ composite oxide onto SBA-16 that showed the higher catalytic performance having a molar Ce:Zr:Sn ratio of 0.68:0.17:0.15. Catalysts were synthesized with different CZSn$_{0,15}$ loading amounts and a constant platinum content of 7 wt%, denoted as Pt7CZSn$_{0.15}$*x*SBA, where *x* indicates the weight percentage of CZSn$_{0,15}$.

The elemental composition and BET surface area are listed in **Table 2.** It was confirmed that increasing the CZSn$_{0.15}$ content led to a progressive decrease in surface area. This reduction suggests successful dispersion and incorporation of CZSn$_{0.15}$ into the SBA-16 framework. At higher loading amounts, CZSn likely filled the mesopores and partially covered the external surface of SBA-16, which reduced the available surface area [29,30].

XRD patterns of the Pt7CZSn$_{0.15}$*x*SBA catalysts are shown in **Fig. 4.** All samples displayed characteristic peaks associated with the mesoporous SBA-16, the cubic fluorite-type CeO_2–ZrO_2–SnO_2 phase, and metallic Pt. Notably, as the CZSn$_{0.15}$ loading increased, the intensity of the fluorite-type diffraction peaks also increased, indicating the presence of a more crystalline CZSn$_{0.15}$ phase.

Table 2 The measured composition and surface area of the prepared 7.0wt% Pt/ *x*wt% $Ce_{0.68}Zr_{0.17}Sn_{0.15}O_2$/ SBA-16 (Pt7CZSn$_{0.15}$*x*SBA) catalysts with different *x*

x	Measured composition	Surface area ($m^2 \cdot g^{-1}$)
10	7.1wt%Pt/9.8wt%$Ce_{0.67}Zr_{0.18}Sn_{0.15}O_2$/SBA-16	290
16	6.8wt%/Pt/16.4wt%$Ce_{0.69}Zr_{0.17}Sn_{0.14}O_2$/SBA-16	283
20	7wt%Pt/20.1wt%$Ce_{0.68}Zr_{0.18}Sn_{0.14}O_2$/SBA-16	216
25	6.9wt%Pt/24.8wt%$Ce_{0.69}Zr_{0.18}Sn_{0.13}O_2$/SBA-16	198

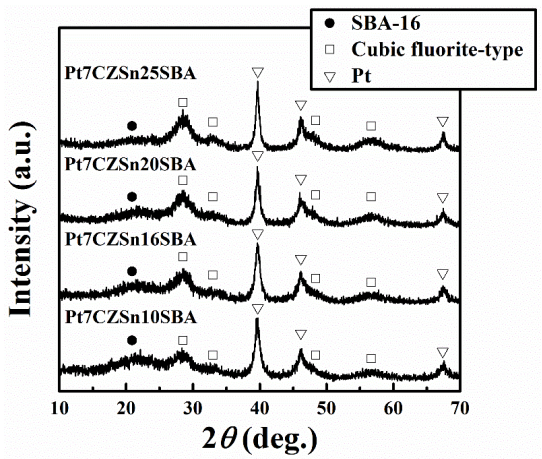

Figure 4 XRD patterns of Pt7CZSn$_{0.15}$*x*SBA catalysts

The Pt7SBA catalyst, without CZSn$_{0.15}$, shows some phenol removal activity due to the ability of Pt to activate molecular oxygen and subsequently oxidize the phenol. Interestingly, the incorporation of CZSn$_{0.15}$ as an oxygen promoter significantly enhanced phenol conversion and suppressed the accumulation of benzoquinone, which is a common intermediate in phenol oxidation [31-32], as shown in **Fig. 5**. This facilitates a more efficient oxidation process, as the CZSn$_{0.15}$ actively participates in oxygen transfer to Pt, leading to improved phenol conversion. As the CZSn content increased up to 16 wt%, catalytic activity improved, attributed to the greater availability of lattice oxygen, which facilitated the oxidation process. However, further increases in CZSn loading beyond 16 wt% led to a decline in catalytic performance. This reduction is likely due to excessive pore blockage and surface coverage of SBA-16 by the dense CZSn phase, resulting in a decreased surface area and limited accessibility to active sites. Catalysts with higher CZSn content also produced lower amounts

of benzoquinone intermediate, suggesting that CZSn enabled deeper oxidation toward final products such as CO_2 or other smaller molecules.

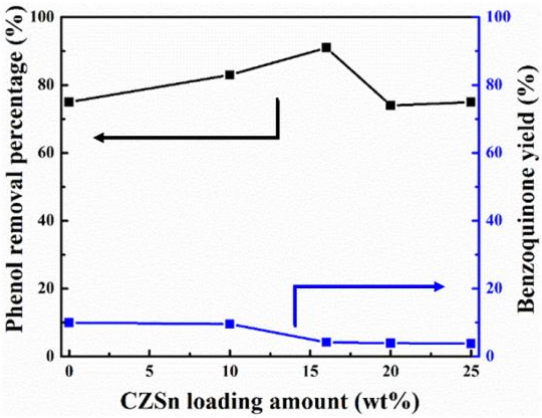

Figure 5 Performance Pt7CZSn$_{0.15}$*x*SBA catalysts with a reference of Pt7SBA (*x* = CZSn$_{0.15}$ loading amount)

3.3 The effect of Pt loading amount on the performance of catalyst

Following the naming convention used above, the catalysts with *y* wt% Pt loaded onto 16 wt% $Ce_{0.68}Zr_{0.17}Sn_{0.15}O_2$/SBA-16 are referred to as Pt*y*CZSn$_{0.15}$16SBA. The XRD patterns of CZSn$_{0.15}$16SBA and Pt*y*CZSn$_{0.15}$16SBA catalysts are presented in **Fig. 6**. No impurity phases were detected, indicating the high purity and successful incorporation of all components. As the Pt loading increased, the diffraction peaks corresponding to metallic Pt became more prominent, indicating improved crystallinity and higher Pt content. This trend also suggests the growth of Pt crystallite size with increasing loading, as evidenced by the sharpening and intensity enhancement of Pt-related peaks.

Table 3 summarizes the actual metal compositions and surface areas of the Pt*y*CZSn16SBA catalysts. The elemental analysis confirmed that the measured compositions closely matched the nominal feed ratios, demonstrating good control over the synthesis. The surface area of the catalysts tended to decrease gradually with increasing Pt content, likely due to partial pore blockage or coverage of SBA-16 by Pt nanoparticles, which may reduce the accessible surface area for reactants **[29,30]**.

The Pt loading effect on the catalytic performance of Pt*y*CZSn$_{0.15}$16SBA (*y* = 0, 1, 3, 7, 10) was evaluated and the results are shown in Fig. 7. The introduction of Pt significantly enhanced the catalytic activity compared to the Pt-free CZSn16SBA, confirming the vital role of Pt as an active site for oxidation. Phenol removal efficiency increased with increasing Pt loading up to 7 wt%, which is attributed to the higher number of available active Pt sites that facilitate the activation of oxygen species for phenol oxidation. However, further increase of Pt loading to 10 wt% led to a decline in catalytic activity. This drop can be correlated with the reduction in surface area, as observed in **Table 3**, likely due to pore blockage or particle agglomeration at higher Pt concentrations. These results indicate that 7 wt% is the optimal Pt loading, offering the best balance between active site availability and surface area for efficient phenol oxidation.

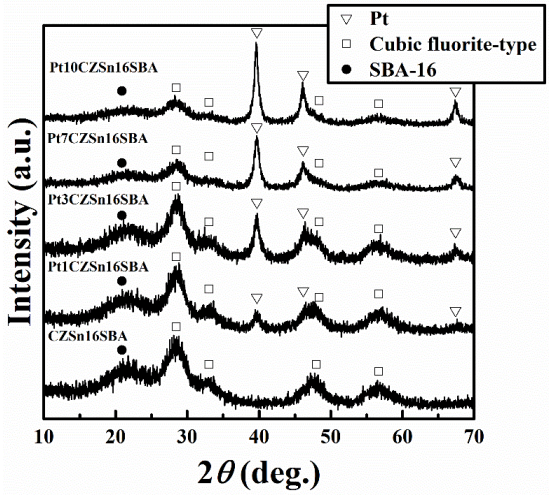

Figure 6 XRD patterns of *y*wt% Pt/ 16wt% $Ce_{0.68}Zr_{0.17}Sn_{0.15}O_2$/ SBA-16 (Pt*y*CZSn$_{0.15}$16SBA) catalysts

Table 3 The measured composition and surface area of the prepared Pt*y*CZSn$_{0.15}$16SBA catalysts

y	Measured composition	Surface area ($m^2 \cdot g^{-1}$)
1	1.2wt%Pt/18.0wt%$Ce_{0.69}Zr_{0.16}Sn_{0.15}O_2$/SBA-16	290
3	3.2wt%Pt/15.3wt%$Ce_{0.65}Zr_{0.18}Sn_{0.17}O_{2.0}$/SBA-16	285
7	6.8wt%Pt/16.4wt%$Ce_{0.69}Zr_{0.17}Sn_{0.14}O_{2.0}$/SBA-16	283
10	9.8wt%Pt/16.3wt%$Ce_{0.67}Zr_{0.18}Sn_{0.15}O_{2.0}$/SBA-16	252

3.4 Kinetic Study of Phenol Oxidation over Pt7CZSn16SBA Catalyst

The reaction temperature effect on the catalytic activity of Pt7CZSn$_{0.15}$16SBA was examined at 60, 70, and 80 °C, under atmospheric pressure for 2-8 hours. As shown in **Fig. 8**, the catalytic performance improved significantly with

increasing temperature, indicating enhanced reaction kinetics at higher thermal energy.

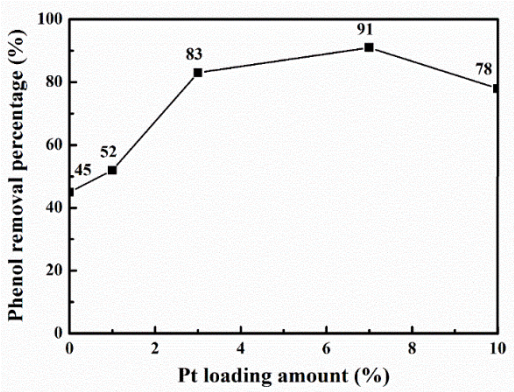

Figure 7 Performance of Pt*y*CZSn$_{0.15}$16SBA catalysts with reference of CZSn16SBA (*y* = Pt loading amount)

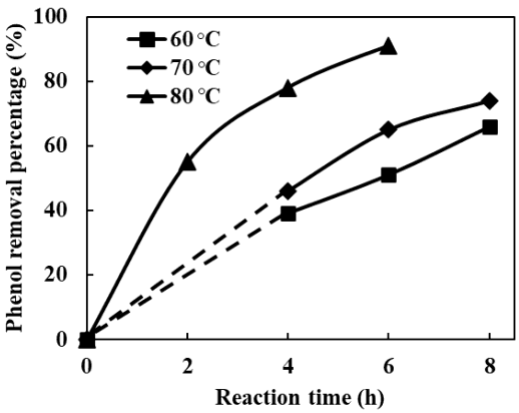

Figure 8 Phenol removal percentage after reaction using Pt7CZSn$_{0.15}$16SBA catalyst at 60, 70, and 80 °C

To further evaluate the reaction kinetics, the concentration–time data were fitted to a pseudo-first-order kinetic model. **Fig. 9** presents the plots of $-\ln(C/C_0)$ versus reaction time at each temperature. The linearity of the plots suggests that phenol oxidation over Pt7CZSn$_{0.15}$16SBA proceeds via pseudo-first-order kinetics, consistent with previous studies on similar systems [14].

Using the slope of each linear plot, the apparent rate constants were calculated based on the first-order rate law. The rate constants for phenol oxidation were determined to be 0,13 h^{-1}, 0,17 h^{-1}, and 0.39 h^{-1} at 60°C, 70°C, and 80°C, respectively. Furthermore, the activation energy (E_a) was estimated from the Arrhenius equation using the rate constants at different temperatures. The corresponding Arrhenius plot (**Fig. 10**) exhibits good linearity, indicating reliable kinetic behavior. The activation energy for phenol oxidation over Pt7CZSn$_{0.15}$16SBA was calculated to be 57.7 kJ·mol^{-1}. This value is lower than the activation energy of cobalt catalyst loaded on various support (59.7–75.5 kJ mol^{-1}) and RuO_2 (61.4 kJ mol^{-1}) or CuO (72.6 kJ mol^{-1}) loaded on activated carbon for phenol removal [33-37]. These findings confirm that the catalyst demonstrates efficient oxidation activity under mild conditions and follows well-defined reaction kinetics.

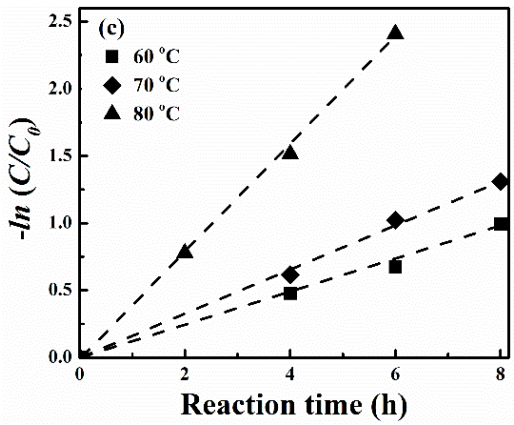

Figure 9 Reaction rate constant of phenol oxidation reaction using Pt7CZSn$_{0.15}$16SBA catalyst

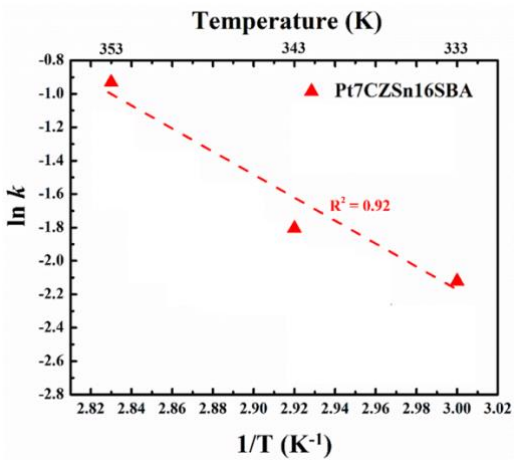

Figure 10 Arrhenius plot phenol oxidation using Pt7CZSn$_{0.15}$16SBA catalyst

4 Conclusion

This study successfully demonstrated the optimization of Pt/CeO_2–ZrO_2–SnO_2/SBA-16 catalysts for phenol oxidation under mild reaction conditions. The optimum SnO_2 content in the CeO_2–ZrO_2–SnO_2 (CZSn) oxygen promoter was found at a molar ratio of 0.15, providing the highest redox activity and phenol removal efficiency. Further, the ideal loading amount of the

CZSn promoter on SBA-16 was determined to be 16 wt%, balancing sufficient oxygen storage capacity and surface area. The optimal platinum loading was 7 wt%, which maximized catalytic activity without excessively blocking the support's porosity. Kinetic studies confirmed that the reaction follows pseudo-first-order kinetics, with a rate constant of 0.39 h^{-1} at 80 °C and an apparent activation energy of 57.7 $kJ \cdot mol^{-1}$. These findings indicate that $Pt7CZSn_{0.15}16SBA$ is a highly effective catalyst for phenol removal via catalytic wet air oxidation, offering promising performance at lower temperature and atmospheric pressure.

Acknowledgement

The authors would like to express their sincere gratitude to Inorganic Material Chemistry Laboratory, Osaka University, for providing access to the laboratory facilities and equipment used in this research. The authors also acknowledge the support from Institut Teknologi Bandung (ITB) through PPMI KK 2025 for the funding provided to complete the preparation and writing of this article.

References

[1] Ayral C., Lebigue CJ., Stüber F., Wilhelm AM., Delmas H., 2010, Catalytic Wet Air Oxidation of Phenolic Compounds and Mixtures over Activated Carbon: Conversion, Mineralization, and Catalyst Stability, *Ind. Eng. Chem. Res.*, 49:10707–10714. https://doi.org/10.1021/ie100240n

[2] Masende ZPG., Kuster BFM., Ptasinski KJ., Janssen FJJG., JHY. Katima, JC. Sxhouten., 2010, Kinetics of malonic acid degradation in aqueous phase over Pt/graphite catalyst, *Appl. Catal. B: Environ.*, 41:247–267. https://doi.org/10.1016/j.apcatb.2004.09.010

[3] Munn SJ., Aschberger K., Cosgrove O., Pakalin S., Paya-Perez A., Schulz BS., Vegro S., *European union risk assessment report: phenol*. 64 revised edition. https://echa.europa.eu/documents/10162/3e04f30d-9953-4824-ba04-defa32a130fa Accessed 17 February 2025

[4] Kulkarni SJ., Kaware JP., 2013, Desorption studies for low cost adsorbents, *Int. Journal of Sci. and Res.*, 3(4): 1–5.

[5] Yang S., Zhu W., Wang J., Chen Z., 2008, Catalytic wet air oxidation of phenol over CeO_2-TiO_2 catalyst in the batch reactor and the packed-bed reactor, *J. Haz. Mat.*, 153:1248–1253. https://doi.org/10.1016/j.jhazmat.2007.09.084

[6] Brown VM., Jordan DHM., Tiller BA., 1967, The effect of temperature on the acute toxicity of phenol to rainbow trout in hard water, *Water. Res.*, 1:587–594. https://doi.org/10.1016/0043-1354(67)90041-3

[7] Chung TP., Tseng HY., Juang RS., 2003, Mass transfer effect and intermediate detection for phenol degradation in immobilized *Pseudomonas putida* systems, *Proc. Biochem.*, 38:1497–1507. https://doi.org/10.1016/s0032-9592(03)00038-4

[8] Kibert M., Somitsch W., Robra KH., 2000, Characterization of a phenol degrading mixed population by enzyme assay, *Wat. Res.*, 34(4):1127–1134. https://doi.org/10.1016/S0043-1354(99)00248-1

[9] de Los Monteros AE., Lafaye G., Cervantes A., Del Angel G., Barbier Jr, J., Torres G. 2015, Catalytic wet air oxidation of phenol over metal catalyst (Ru, Pt) supported on TiO_2–CeO_2 oxides, *Catalysis Today*, *258*, 564-569. https://dx.doi.org/10.1016/j.cattod.2015.01.009

[10] Keav S., Martin A., Barbier Jr J., Duprez D., 2010, Deactivation and reactivation of noble metal catalysts tested in the Catalytic Wet Air Oxidation of phenol, *Catalysis Today*, *151*(1-2), 143-147. https://doi.org/10.1016/j.cattod.2010.01.025

[11] Keav S., de Los Monteros AE., Barbier Jr J., Duprez D., 2014, Wet Air Oxidation of phenol over Pt and Ru catalysts supported on cerium-based oxides: Resistance to fouling and kinetic modelling, *Applied Catalysis B: Environmental*, *150*, 402-410. https://dx.doi.org/10.1016/j.apcatb.2013.12.028

[12] Nousir S., Keav S., Barbier Jr J., Bensitel M., Brahmi R., Duprez D., 2008, Deactivation phenomena during catalytic wet air oxidation (CWAO) of phenol over platinum catalysts supported on ceria and ceria–zirconia mixed oxides. *Applied Catalysis B:*

Environmental, *84*(3-4), 723-731. https://doi.org/10.1016/j.apcatb.2008.06.010

[13] Guo J., Al-Dahhan M., 2003, Catalytic wet oxidation of phenol by hydrogen peroxide over pillared clay catalyst. *Industrial & engineering chemistry research*, *42*(12), 2450-2460. https://doi.org/10.1021/ie020344t

[14] Muhammad S., Saputra E., Sun H., Ang H. M., Tadé MO., Wang S., 2012, Heterogeneous catalytic oxidation of aqueous phenol on red mud-supported cobalt catalysts. *Industrial & engineering chemistry research*, *51*(47), 15351-15359. https://doi.org/10.1021/ie301639t

[15] Bedrane S., Descorme C., Duprez D., 2002, Investigation of the oxygen storage process on ceria-and ceria–zirconia-supported catalysts, *Catalysis Today*, *75*(1-4), 401-405. https://dx.doi.org/10.1016/s0920-5861(02)00089-5

[16] Fornasiero P., Dimonte R., Rao GR., Kaspar J., Meriani S., Trovarelli AO., Graziani M., 1995, Rh-loaded CeO_2-ZrO_2 solid-solutions as highly efficient oxygen exchangers: dependence of the reduction behavior and the oxygen storage capacity on the structural-properties, *Journal of Catalysis*, *151*(1), 168-177. https://doi.org/10.1006/jcat.1995.1019

[17] Hori CE., Permana H., Ng KS., Brenner A., More K., Rahmoeller KM., Belton D., 1998, Thermal stability of oxygen storage properties in a mixed CeO_2-ZrO_2 system, *Applied Catalysis B: Environmental*, *16*(2), 105-117. https://doi.org/10.1016/S0926-3373(97)00060-X

[18] Kašpar, J., Fornasiero, P., & Graziani, M., 1999, Use of CeO_2-based oxides in the three-way catalysis. *Catalysis Today*, *50*(2), 285-298. https://doi.org/10.1016/S0920-5861(98)00510-0

[19] Yasuda, K., Yoshimura, A., Katsuma, A., Masui, T., & Imanaka, N., 2012, Low-temperature complete combustion of volatile organic compounds over novel Pt/CeO_2–ZrO_2–SnO_2/γ-Al_2O_3 catalysts. *Bulletin of the Chemical Society of Japan*, *85*(4), 522-526. https://doi.org/10.1246/bcsj.20110382

[20] Dong, Q., Yin, S., Guo, C., & Sato, T., 2012, $Ce_{0.5}Zr_{0.4}Sn_{0.1}O_2/Al_2O_3$ catalysts with enhanced oxygen storage capacity and high CO oxidation activity. *Catalysis Science & Technology*, *2*(12), 2521-2524. https://doi.org/10.1039/C2CY20425H

[21] Supandi, A. R., Nunotani, N., & Imanaka, N., 2017, Liquid-phase oxidation of phenol in facile condition using Pt/CeO_2–ZrO_2–SnO_2 catalyst supported on mesoporous silica SBA-16. *Journal of environmental chemical engineering*, *5*(4), 3999-4003. https://doi.org/10.1080/21870764.2020.1786238

[22] Zhao, D., Huo, Q., Feng, J., Chmelka, B. F., & Stucky, G. D., 1998, Nonionic triblock and star diblock copolymer and oligomeric surfactant syntheses of highly ordered, hydrothermally stable, mesoporous silica structures. *Journal of the American Chemical Society*, *120*(24), 6024-6036. https://doi.org/10.1021/ja974025i

[23] Yotou, H., Okamoto, T., Ito, M., Sekino, T., & Tanaka, S. I., 2013, Novel method for insertion of Pt/$CeZrO_2$ nanoparticles into mesoporous SBA-16 using hydrothermal treatment. *Applied Catalysis A: General*, *458*, 137-144. https://doi.org/10.1016/j.apcata.2013.03.025

[24] Shannon, R. D., 1976, Revised effective ionic radii and systematic studies of interatomic distances in halides and chalcogenides. *Foundations of Crystallography*, *32*(5), 751-767.

[25] Ayastuy, J. L., Iglesias-González, A., & Gutiérrez-Ortiz, M. A., 2014, Synthesis and characterization of low amount tin-doped ceria ($Ce_xSn_{1-x}O_{2-\delta}$) for catalytic CO oxidation. *Chemical Engineering Journal*, *244*, 372-381. https://doi.org/10.1016/j.cej.2014.01.077

[26] Yao, X., Tang, C., Ji, Z., Dai, Y., Cao, Y., Gao, F., ... & Chen, Y., 2013, Investigation of the physicochemical properties and catalytic activities of $Ce_{0.67}M_{0.33}O_2$ (M= Zr^{4+}, Ti^{4+}, Sn^{4+}) solid solutions for NO removal by CO. *Catalysis Science & Technology*, *3*(3), 688-698. https://doi.org/10.1039/C2CY20610B

[27] Baidya, T., Dutta, G., Hegde, M. S., & Waghmare, U. V., 2009, Noble metal ionic catalysts: correlation of increase in CO oxidation activity with increasing effective charge on Pd ion in Pd ion substituted $Ce_{1-x}M_xO_{2-\delta}$ (M= Ti, Zr and Hf). *Dalton Transactions*, (3), 455-464. https://doi.org/10.1039/B814742F

[28] Baidya, T., Gupta, A., Deshpandey, P. A., Madras, G., & Hegde, M. S. (2009). High

Oxygen Storage Capacity and High Rates of CO Oxidation and NO Reduction Catalytic Properties of $Ce_{1-x}Sn_xO_2$ and $Ce_{0.78}Sn_{0.2}Pd_{0.02}O_{2-\delta}$. *The Journal of Physical Chemistry C*, *113*(10), 4059-4068. http://dx.doi.org/10.1021/jp8060569

[29] Enumula, S. S., Gurram, V. R. B., Kondeboina, M., Burri, D. R., & Kamaraju, S. R. R., 2016, ZrO_2/SBA-15 as an efficient catalyst for the production of γ-valerolactone from biomass-derived levulinic acid in the vapour phase at atmospheric pressure. *RSC Advances*, *6*(24), 20230-20239. https://doi.org/10.1039/C5RA27513J

[30] Melero, J. A., Moreno, J., Iglesias, J., Morales, G., Fierro, J. L. G., Sánchez-Vázquez, R., ... & García, B., 2020, Ru-ZrO_2-SBA-15 as efficient and robust catalyst for the aqueous phase hydrogenation of glucose to sorbitol. *Molecular Catalysis*, *484*, 110802. https://doi.org/10.1016/j.mcat.2020.110802

[31] Cui, R., Zhang, Q., Zhao, B., & Tang, Z., 2025, Catalytic wet air oxidation of phenol in wastewater over Ru catalysts supported on La doped TiO_2: Improvements on activity and stability. *Journal of Water Process Engineering*, *70*, 107060. https://doi.org/10.1016/j.jwpe.2025.107060

[32] Izquierdo-Colorado, A., Torres-Torres, G., Gamboa-Rodríguez, M. T., Silahua-Pavón, A. A., Arévalo-Pérez, J. C., Cervantes-Uribe, A., ... & Beltramini, J. N., 2019, Catalytic Wet Air Oxidation (CWAO) of Phenol in a Fixed Bed Reactor Using Supported Ru and Ru-Au Catalysts: Effect of Gold and Ce Loading. *ChemistrySelect*, *4*(4), 1275-1284. https://doi.org/10.1002/slct.201802958

[33] Shukla, P., Wang, S., Singh, K., Ang, H. M., & Tadé, M. O., 2010, Cobalt exchanged zeolites for heterogeneous catalytic oxidation of phenol in the presence of peroxymonosulphate. *Applied Catalysis B: Environmental*, *99*(1-2), 163-169. https://doi.org/10.1016/j.apcatb.2010.06.013

[34] Shukla, P. R., Wang, S., Sun, H., Ang, H. M., & Tadé, M., 2010, Activated carbon supported cobalt catalysts for advanced oxidation of organic contaminants in aqueous solution. *Applied Catalysis B: Environmental*, *100*(3-4), 529-534. https://doi.org/10.1016/j.apcatb.2010.09.006

[35] Shukla P., Sun H., Wang S., Ang HM., Tadé, MO.,2011, Nanosized Co_3O_4/SiO_2 for heterogeneous oxidation of phenolic contaminants in waste water, *Separation and Purification Technology*, *77*(2), 230-236. https://doi.org/10.1016/j.seppur.2010.12.011

[36] Muhammad S., Shukla PR., Tadé MO., Wang, S., 2012, Heterogeneous activation of peroxymonosulphate by supported ruthenium catalysts for phenol degradation in water, *Journal of Hazardous Materials*, *215*, 183-190. https://doi.org/10.1016/j.jhazmat.2012.02.045

[37] Álvarez PM., McLurgh D., Plucinski P., 2002, Copper oxide mounted on activated carbon as catalyst for wet air oxidation of aqueous phenol, 2. Catalyst stability. *Industrial & engineering chemistry research*, *41*(9), 2153-2158.